Properties of a New Group of Cosmic Nuclei: Results from the Alpha Magnetic Spectrometer on Sodium, Aluminum, and Nitrogen

M. Aguilar,[29] L. Ali Cavasonza,[1] B. Alpat,[36] G. Ambrosi,[36] L. Arruda,[27] N. Attig,[24] F. Barao,[27] L. Barrin,[15] A. Bartoloni,[42] S. Başeğmez-du Pree,[18,*] R. Battiston,[39,40] M. Behlmann,[10] B. Beranek,[1] J. Berdugo,[29] B. Bertucci,[36,37] V. Bindi,[20] K. Bollweg,[21] B. Borgia,[42,43] M. J. Boschini,[31] M. Bourquin,[16] E. F. Bueno,[18] J. Burger,[10] W. J. Burger,[39] S. Burmeister,[25] X. D. Cai,[10] M. Capell,[10] J. Casaus,[29] G. Castellini,[14] F. Cervelli,[38] Y. H. Chang,[47] G. M. Chen,[6,7] G. R. Chen,[23] H. S. Chen,[6,7] Y. Chen,[16,23] L. Cheng,[23] H. Y. Chou,[48] S. Chouridou,[1] V. Choutko,[10] C. H. Chung,[1] C. Clark,[10,21] G. Coignet,[3] C. Consolandi,[20] A. Contin,[8,9] C. Corti,[20] Z. Cui,[22,23] K. Dadzie,[10] C. Delgado,[29] S. Della Torre,[31] M. B. Demirköz,[2] L. Derome,[17] S. Di Falco,[38] V. Di Felice,[44,†] C. Díaz,[29] F. Dimiccoli,[39] P. von Doetinchem,[20] F. Dong,[34] F. Donnini,[44,†] M. Duranti,[36] A. Egorov,[10] A. Eline,[10] J. Feng,[10] E. Fiandrini,[36,37] P. Fisher,[10] V. Formato,[44,†] C. Freeman,[20] C. Gámez,[29] R. J. García-López,[26] C. Gargiulo,[15] H. Gast,[1] M. Gervasi,[31,32] F. Giovacchini,[29] D. M. Gómez-Coral,[20] J. Gong,[34] C. Goy,[3] V. Grabski,[30] D. Grandi,[31,32] M. Graziani,[36,37] S. Haino,[47] K. C. Han,[28] R. K. Hashmani,[2] Z. H. He,[19] B. Heber,[25] T. H. Hsieh,[10] J. Y. Hu,[6,7] M. Incagli,[38] W. Y. Jang,[13] Yi Jia,[10] H. Jinchi,[28] B. Khiali,[44,†] G. N. Kim,[13] Th. Kirn,[1] M. Konyushikhin,[10] O. Kounina,[10] A. Kounine,[10] V. Koutsenko,[10] D. Krasnopevtsev,[10] A. Kuhlman,[20] A. Kulemzin,[10] G. La Vacca,[31,32] E. Laudi,[15] G. Laurenti,[8] I. Lazzizzera,[39,40] A. Lebedev,[10] H. T. Lee,[46] S. C. Lee,[47] J. Q. Li,[34] M. Li,[1] Q. Li,[34] S. Li,[1] J. H. Li,[22] Z. H. Li,[6,7] J. Liang,[22] C. Light,[20] C. H. Lin,[47] T. Lippert,[24] J. H. Liu,[5] Z. Liu,[16] S. Q. Lu,[47] Y. S. Lu,[6] K. Luebelsmeyer,[1] J. Z. Luo,[34] Xi Luo,[23] F. Machate,[1] C. Mañá,[29] J. Marín,[29] J. Marquardt,[25] T. Martin,[10,21] G. Martínez,[29] N. Masi,[8,9] D. Maurin,[17] A. Menchaca-Rocha,[30] Q. Meng,[34] V. V. Mikhailov,[33] M. Molero,[29] P. Mott,[10,21] L. Mussolin,[36,37] J. Negrete,[20] N. Nikonov,[1] F. Nozzoli,[39] A. Oliva,[8] M. Orcinha,[27] M. Palermo,[20] F. Palmonari,[8,9] M. Paniccia,[16] A. Pashnin,[10] M. Pauluzzi,[36,37] S. Pensotti,[31,32] H. D. Phan,[10] V. Plyaskin,[10] M. Pohl,[16] S. Poluianov,[35] X. Qin,[10] Z. Y. Qu,[47] L. Quadrani,[8,9] P. G. Rancoita,[31] D. Rapin,[16] A. Reina Conde,[26] E. Robyn,[16] S. Rosier-Lees,[3] A. Rozhkov,[10] D. Rozza,[31,32] R. Sagdeev,[11] S. Schael,[1] A. Schulz von Dratzig,[1] G. Schwering,[1] E. S. Seo,[12] Z. Shakfa,[2] B. S. Shan,[4] T. Siedenburg,[1] C. Solano,[10] J. W. Song,[22] X. J. Song,[23] R. Sonnabend,[1] L. Strigari,[42,‡] T. Su,[23] Q. Sun,[22] Z. T. Sun,[6,7] M. Tacconi,[31,32] X. W. Tang,[6] Z. C. Tang,[6] J. Tian,[36,37] Samuel C. C. Ting,[10,15] S. M. Ting,[10] N. Tomassetti,[36,37] J. Torsti,[49] C. Türsüz,[2] T. Urban,[10,21] I. Usoskin,[35] V. Vagelli,[41,36] R. Vainio,[49] M. Valencia-Otero,[48] E. Valente,[42,43] E. Valtonen,[49] M. Vázquez Acosta,[26] M. Vecchi,[18] M. Velasco,[29] J. P. Vialle,[3] C. X. Wang,[22] L. Wang,[5] L. Q. Wang,[22] N. H. Wang,[22] Q. L. Wang,[5] S. Wang,[20] X. Wang,[10] Yu Wang,[22] Z. M. Wang,[23] J. Wei,[16] Z. L. Weng,[10] H. Wu,[34] R. Q. Xiong,[34] W. Xu,[22,23] Q. Yan,[10] Y. Yang,[45] I. I. Yashin,[33] H. Yi,[34] Y. M. Yu,[10] Z. Q. Yu,[6] M. Zannoni,[31,32] C. Zhang,[6] F. Zhang,[6] F. Z. Zhang,[6,7] J. H. Zhang,[34] Z. Zhang,[10] F. Zhao,[6,7] C. Zheng,[23] Z. M. Zheng,[4] H. L. Zhuang,[6] V. Zhukov,[1] A. Zichichi,[8,9] and P. Zuccon[39,40]

(AMS Collaboration)

[1]I. Physics Institute and JARA-FAME, RWTH Aachen University, 52056 Aachen, Germany
[2]Department of Physics, Middle East Technical University (METU), 06800 Ankara, Turkey
[3]Université Grenoble Alpes, Université Savoie Mont Blanc, CNRS, LAPP-IN2P3, 74000 Annecy, France
[4]Beihang University (BUAA), Beijing 100191, China
[5]Institute of Electrical Engineering (IEE), Chinese Academy of Sciences, Beijing 100190, China
[6]Institute of High Energy Physics (IHEP), Chinese Academy of Sciences, Beijing 100049, China
[7]University of Chinese Academy of Sciences (UCAS), Beijing 100049, China
[8]INFN Sezione di Bologna, 40126 Bologna, Italy
[9]Università di Bologna, 40126 Bologna, Italy
[10]Massachusetts Institute of Technology (MIT), Cambridge, Massachusetts 02139, USA
[11]East-West Center for Space Science, University of Maryland, College Park, Maryland 20742, USA
[12]IPST, University of Maryland, College Park, Maryland 20742, USA
[13]CHEP, Kyungpook National University, 41566 Daegu, Korea
[14]CNR–IROE, 50125 Firenze, Italy
[15]European Organization for Nuclear Research (CERN), 1211 Geneva 23, Switzerland
[16]DPNC, Université de Genève, 1211 Genève 4, Switzerland
[17]Université Grenoble Alpes, CNRS, Grenoble INP, LPSC-IN2P3, 38000 Grenoble, France
[18]Kapteyn Astronomical Institute, University of Groningen, P.O. Box 800, 9700 AV Groningen, Netherlands

[19]Sun Yat-Sen University (SYSU), Guangzhou 510275, China

[20]Physics and Astronomy Department, University of Hawaii, Honolulu, Hawaii 96822, USA

[21]National Aeronautics and Space Administration Johnson Space Center (JSC), Houston, Texas 77058, USA

[22]Shandong University (SDU), Jinan, Shandong 250100, China

[23]Shandong Institute of Advanced Technology (SDIAT), Jinan, Shandong 250100, China

[24]Jülich Supercomputing Centre and JARA-FAME, Research Centre Jülich, 52425 Jülich, Germany

[25]Institut für Experimentelle und Angewandte Physik, Christian-Alberts-Universität zu Kiel, 24118 Kiel, Germany

[26]Instituto de Astrofísica de Canarias (IAC), 38205 La Laguna, and Departamento de Astrofísica, Universidad de La Laguna, 38206 La Laguna, Tenerife, Spain

[27]Laboratório de Instrumentação e Física Experimental de Partículas (LIP), 1649-003 Lisboa, Portugal

[28]National Chung–Shan Institute of Science and Technology (NCSIST), Longtan, Tao Yuan 32546, Taiwan

[29]Centro de Investigaciones Energéticas, Medioambientales y Tecnológicas (CIEMAT), 28040 Madrid, Spain

[30]Instituto de Física, Universidad Nacional Autónoma de México (UNAM), Ciudad de México, 01000 Mexico

[31]INFN Sezione di Milano–Bicocca, 20126 Milano, Italy

[32]Università di Milano–Bicocca, 20126 Milano, Italy

[33]NRNU MEPhI (Moscow Engineering Physics Institute), Moscow, 115409 Russia

[34]Southeast University (SEU), Nanjing, 210096, China

[35]Sodankylä Geophysical Observatory and Space Physics and Astronomy Research Unit, University of Oulu, 90014 Oulu, Finland

[36]INFN Sezione di Perugia, 06100 Perugia, Italy

[37]Università di Perugia, 06100 Perugia, Italy

[38]INFN Sezione di Pisa, 56100 Pisa, Italy

[39]INFN TIFPA, 38123 Povo, Trento, Italy

[40]Università di Trento, 38123 Povo, Trento, Italy

[41]Agenzia Spaziale Italiana (ASI), 00133 Roma, Italy

[42]INFN Sezione di Roma 1, 00185 Roma, Italy

[43]Università di Roma La Sapienza, 00185 Roma, Italy

[44]INFN Sezione di Roma Tor Vergata, 00133 Roma, Italy

[45]National Cheng Kung University, Tainan 70101, Taiwan

[46]Academia Sinica Grid Center (ASGC), Nankang, Taipei 11529, Taiwan

[47]Institute of Physics, Academia Sinica, Nankang, Taipei 11529, Taiwan

[48]Physics Department and Center for High Energy and High Field Physics, National Central University (NCU), Tao Yuan 32054, Taiwan

[49]Space Research Laboratory, Department of Physics and Astronomy, University of Turku, 20014 Turku, Finland

We report the properties of sodium (Na) and aluminum (Al) cosmic rays in the rigidity range 2.15 GV to 3.0 TV based on 0.46 million sodium and 0.51 million aluminum nuclei collected by the Alpha Magnetic Spectrometer experiment on the International Space Station. We found that Na and Al, together with nitrogen (N), belong to a distinct cosmic ray group. In this group, we observe that, similar to the N flux, both the Na flux and Al flux are well described by the sums of a primary cosmic ray component (proportional to the silicon flux) and a secondary cosmic ray component (proportional to the fluorine flux). The fraction of the primary component increases with rigidity for the N, Na, and Al fluxes and becomes dominant at the highest rigidities. The Na/Si and Al/Si abundance ratios at the source, 0.036 ± 0.003 for Na/Si and 0.103 ± 0.004 for Al/Si, are determined independent of cosmic ray propagation.

Sodium and aluminum cosmic rays, like nitrogen, are thought to be produced both in astrophysical sources and by the collisions of heavier nuclei with the interstellar

medium [1]. Previously, measurements of the cosmic nitrogen flux with the Alpha Magnetic Spectrometer experiment (AMS) have been reported [2,3]. Remarkably, the nitrogen flux is well described over the entire rigidity range by the sum of a primary component (proportional to the oxygen flux [3,4]) and a secondary component (proportional to the boron flux [3,5]). Recently, AMS also reported the properties of primary heavy Ne, Mg, and Si fluxes [3,6] and the secondary F flux [7]. The AMS results revealed that there are

two classes of primary cosmic rays, He-C-O and Ne-Mg-Si. They also revealed that there are two classes of secondary cosmic rays, Li-Be-B and F.

Over the past 50 years, a few cosmic ray experiments have measured the Na and Al fluxes in kinetic energy [8–14]. The measurement errors exceed 50% at ~50 GeV/n (~100 GV in rigidity). There are no measurements of the Na and Al fluxes in rigidity. Precise knowledge of the rigidity dependence of the Na, Al, and N fluxes will provide important insights on cosmic ray production and propagation.

In this Letter we report the precise measurement of the Na and Al fluxes in cosmic rays in the rigidity range from 2.15 GV to 3.0 TV based on 0.46 million sodium and 0.51 million aluminum nuclei collected by AMS during the first 8.5 years (May 19, 2011 to October 30, 2019) of operation aboard the International Space Station. The total flux errors at 100 GV are 5.0% for Na and 4.8% for Al.

Detector.—The layout and description of the AMS detector are presented in Refs. [3,15] and shown in Fig. S1 of the Supplemental Material (SM) [16]. The key elements used in this measurement are the permanent magnet [17], the nine layers, $L1 - L9$, of the silicon tracker [18–20] and the four planes of the time of flight (TOF) scintillation counters [21]. Further information on the AMS layout, performance, trigger and the Monte Carlo (MC) simulations [22,23] is detailed in the SM [16].

Event selection.—In the first 8.5 years AMS has collected 1.50×10^{11} cosmic ray events. Na and Al events are required to be downward going and to have a reconstructed track in the inner tracker, see Fig. S2 of the SM [16] for a reconstructed sodium event. Details of the event selection are contained in the SM [16] and in Refs. [24–28].

With this selection, the charge confusion from noninteracted nuclei (Ne, Mg, and Si) due to the finite AMS charge resolution is negligible, $< 0.5\%$ over the whole rigidity range, see Fig. S3 of the SM [16].

The main source of background comes from heavier nuclei, such as Mg and Si, which interact above tracker $L2$. The background resulting from interactions in the material between $L1$ and $L2$ (transition radiation detector and upper TOF) is evaluated by fitting the charge distribution of tracker $L1$ with charge distribution templates of Ne, Na, Mg, Al, and Si. Then cuts are applied on the $L1$ charge as shown in Fig. S4 of the SM [16]. The charge distribution templates are obtained using $L2$. These templates contain only noninteracting events by requiring that $L1$ and $L3 - L8$ measure the same charge value. This background varies smoothly from 8% below 10 GV to 25% at 3 TV for Na and from 9% below 10 GV to 16% at 3 TV for Al. The uncertainty of this background was obtained by taking into account the statistical and systematic uncertainties in the template fit, see Fig. S4 of the SM [16]. The background from interactions on materials above $L1$ (thin support structures made by carbon fiber and aluminum honeycomb)

has been obtained and its uncertainty was estimated from simulation using MC samples generated according to AMS flux measurements. The simulation of nuclear interactions has been validated with data using nuclear charge changing cross sections (Mg → Na + X, Si → Na + X and Si → Al + X) [23] measured by AMS, as shown in Fig. S5 of the SM [16] together with the background and its uncertainties as functions of rigidity.

After background subtraction we obtain 0.46×10^6 Na and 0.51×10^6 Al nuclei. The overall uncertainty due to background subtraction was obtained by taking in quadrature the uncertainties of two backgrounds described above. It is 1.5% at 2 GV, 1.5% at 100 GV, and 6% at 3.0 TV for Na, and 1% at 2 GV, 1.5% at 100 GV, and 5% at 3.0 TV for Al.

Data analysis.—The isotropic flux Φ_i in the ith rigidity bin $(R_i, R_i + \Delta R_i)$ is given by

$$\Phi_i = \frac{N_i}{A_i \epsilon_i T_i \Delta R_i}, \tag{1}$$

where N_i is the number of events corrected for bin-to-bin migration, A_i is the effective acceptance, ϵ_i is the trigger efficiency, and T_i is the collection time. In this Letter the flux was measured in 49 bins from 2.15 GV to 3.0 TV, with bin widths chosen according to the rigidity resolution and available statistics.

The bin-to-bin migration of events was corrected using the unfolding procedure described in Ref. [25]. These corrections, $(N_i - \aleph_i)/\aleph_i$ where $\aleph_i$ is the number of observed events in bin i, are +20% at 3 GV decreasing smoothly to +6% at 10 GV, −1% at 100 GV, −10% at 300 GV, and −20% at 3.0 TV for Na and similar for Al.

Extensive studies were made of the systematic errors. These errors include the uncertainties in the background evaluation discussed above, the trigger efficiency, the geomagnetic cutoff factor, the acceptance calculation, the rigidity resolution function, and the absolute rigidity scale.

The systematic error on the fluxes associated with the trigger efficiency measurement is $< 1\%$ over the entire rigidity range.

The geomagnetic cutoff factor was varied from 1.0 to 1.4, resulting in a negligible systematic uncertainty ($<0.1\%$) in the rigidity range below 30 GV.

The effective acceptances A_i were calculated using MC simulation and corrected for small differences between the data and simulated events related to (i) event reconstruction and selection, namely, in the efficiencies of velocity vector determination, track finding, charge determination, and tracker quality cuts and (ii) the details of inelastic interactions of nuclei in the AMS materials. The total corrections to the effective acceptance from the differences between data and MC simulation were found to be $< 5\%$ over the entire rigidity range. The systematic

errors on the fluxes associated with the reconstruction and selection are $<1\%$ over the entire rigidity range.

The material traversed by nuclei from the top of AMS to $L9$ is composed primarily of carbon and aluminum. The survival probabilities of Na and Al nuclei due to interactions in the materials were evaluated using cosmic ray data collected by AMS as described in Ref. [23]. The systematic error due to uncertainties in the evaluation of the inelastic cross section is $<3.5\%$ up to 100 GV. Above 100 GV, the small rigidity dependence of the cross section from the Glauber-Gribov model [22] was treated as an uncertainty and added in quadrature to the uncertainties from the measured interaction probabilities [23]. The corresponding systematic error on both the Na and Al fluxes is $<3.5\%$ up to 100 GV and rises smoothly to 4% at 3.0 TV.

The rigidity resolution functions for Na and Al have pronounced Gaussian cores characterized by widths σ and non-Gaussian tails more than 2.5σ away from the center [24]. The systematic error on the fluxes due to the rigidity resolution function was obtained by repeating the unfolding procedure while varying the width of the Gaussian cores of the resolution functions by 5% and by independently varying the amplitudes of the non-Gaussian tails by 10% [24]. The resulting systematic error is 3.5% at 2 GV, $<1\%$ from 3 GV to 300 GV for both Na and Al fluxes and increases smoothly to 5% for Na and 4% for Al at 3.0 TV.

There are two contributions to the systematic uncertainty on the rigidity scale [3,25]. The first is due to time dependent residual tracker misalignment. This error was estimated by comparing the E/p ratio for electrons and positrons, where E is the energy measured with the electromagnetic calorimeter and p is the momentum measured with the tracker. It was found to be $1/30$ TV^{-1} [29]. The corresponding errors on Na and Al fluxes were obtained by repeating the unfolding procedure with rigidity scale shifts of $\pm 1/30$ TV^{-1} and amount to $<0.4\%$ up to 100 GV for both fluxes increasing to 7% for Na and 6% for Al at 3.0 TV. The second systematic error on the rigidity scale arises from the magnetic field map measurement and its temperature corrections [25]. This amounts to an uncertainty of $<0.6\%$ for both fluxes over the entire rigidity range. The overall error due to uncertainty on the rigidity scale is $<1\%$ up to 200 GV for both Na and Al fluxes and increases smoothly to 7% for Na and 6% for Al at 3.0 TV.

Most importantly, several independent analyses were performed on the same data sample by different study groups. The results of those analyses are consistent with this Letter.

Results.—The measured Na flux Φ_{Na} including statistical and systematic errors is reported in Table SI of the SM [16] as a function of the rigidity at the top of the AMS detector. Figure 1(a) shows the Na flux as a function of rigidity $\tilde{R}$ with the total errors, together with the AMS N flux [3]. In this and subsequent figures the data points are placed along the abscissa at $\tilde{R}$ calculated for a flux $\propto R^{-2.7}$ [30]. The measured Al flux Φ_{Al} including statistical and systematic errors is reported in Table SII of the SM [16] as a function of the rigidity at the top of the AMS detector. Figure 1(b) shows the Al flux as a function of rigidity $\tilde{R}$ with the total errors together with the AMS N flux.
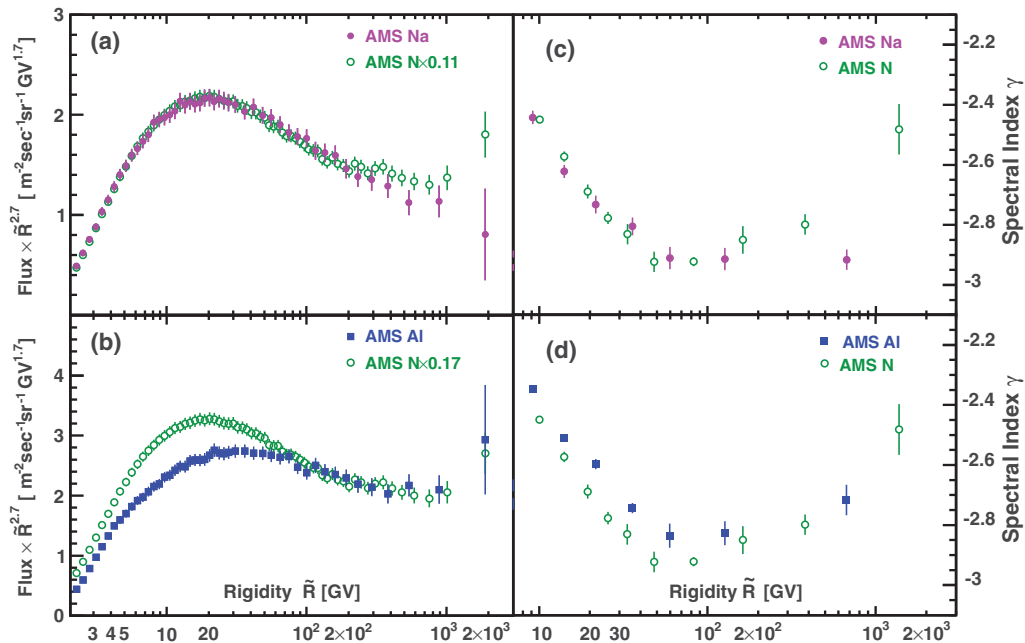

FIG. 1.   As functions of rigidity, the AMS (a) sodium (Na) and (b) aluminum (Al) fluxes together with the rescaled AMS nitrogen (N) flux [3] multiplied by $\tilde{R}^{2.7}$ with total errors; (c) Na and (d) Al flux spectral indices together with the N flux spectral index.

To examine the rigidity dependence of the Na and Al fluxes, the variation of the flux spectral indices with rigidity was obtained in a model independent way from $\gamma = d[\log(\Phi)]/d[\log(R)]$ over nonoverlapping rigidity intervals with a variable width to have sufficient sensitivity to determine γ. The interval boundaries are 7.09, 12.0, 16.6, 28.8, 45.1, 80.5, 211.0, and 3000.0 GV. The results are presented in Figs. 1(c) and 1(d) in comparison with N [3]. As seen from Fig. 1, below $\sim$100 GV, the Na flux and spectral index follow the N flux and spectral index and, above $\sim$100 GV, the Al flux and spectral index follow the N flux and spectral index.

Figure 2 shows the AMS sodium and aluminum fluxes as a function of kinetic energy per nucleon E_K together with earlier measurements [8–13]. Data from other experiments have been extracted using Ref. [31]. Also shown in the figure are the predictions of the latest GALPROP–HELMOD

cosmic ray propagation model [32] based on published AMS data on the two primary cosmic ray classes, He-C-O and Ne-Mg-Si and other AMS data. Note that the GALPROP–HELMOD model agrees well with the AMS aluminum data above 3 GeV/n.

To examine the difference in the rigidity dependence of the sodium and aluminum fluxes with respect to the fluxes of heavy primary cosmic rays, we use the silicon flux Φ_{Si} [6] as a characteristic primary flux. The sodium to silicon flux ratio Φ_{Na}/Φ_{Si} and the aluminum to silicon flux ratio Φ_{Al}/Φ_{Si} were computed and are reported in Tables SIII and SIV of the SM [16], respectively, as functions of rigidity with statistical and systematic errors.
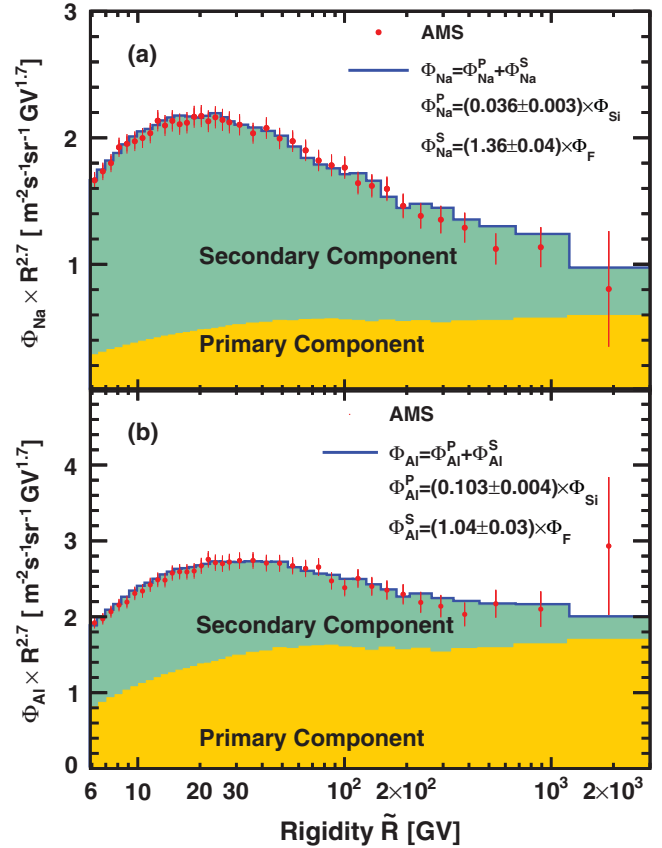

FIG. 2. The AMS (a) sodium flux Φ_{Na} and (b) aluminum flux Φ_{Al} as functions of kinetic energy per nucleon E_K multiplied by $E_K^{2.7}$ together with earlier measurements [8–13]. For the AMS measurements $E_K = (\sqrt{Z^2\tilde{R}^2 + M^2} - M)/A$ where Z, M, and A are the $^{23}_{11}$Na and $^{27}_{13}$Al nuclear charges, masses, and atomic mass numbers, respectively. The dashed blue lines show predictions of the latest GALPROP–HELMOD [32] model based on published AMS data on two primary cosmic ray classes, He-C-O and Ne-Mg-Si and other AMS data. Note the latest GALPROP–HELMOD model agrees well with the AMS aluminum data above 3 GeV/n.

FIG. 3. (a) The AMS sodium flux Φ_{Na} fit to the weighted sum of the silicon flux Φ_{Si} and the fluorine flux Φ_F above 6 GV, i.e., $\Phi_{Na} = \Phi_{Na}^P + \Phi_{Na}^S$. The fit yields $\Phi_{Na}^P = (0.036 \pm 0.003) \times \Phi_{Si}$ and $\Phi_{Na}^S = (1.36 \pm 0.04) \times \Phi_F$ with a $\chi^2/\text{DOF} = 19/36$. (b) The AMS aluminum flux Φ_{Al} fit to the weighted sum of the silicon flux Φ_{Si} and the fluorine flux Φ_F above 6 GV, i.e., $\Phi_{Al} = \Phi_{Al}^P + \Phi_{Al}^S$. The fit yields $\Phi_{Al}^P = (0.103 \pm 0.004) \times \Phi_{Si}$ and $\Phi_{Al}^S = (1.04 \pm 0.03) \times \Phi_F$ with $\chi^2/\text{DOF} = 24/36$. In both (a) and (b), the contributions of the primary and secondary components are indicated by the shading (yellow and green, respectively). As seen, with increasing rigidity, the contributions of the secondary component in both the sodium and aluminum fluxes decrease and the contributions of the primary component correspondingly increase.

TABLE I. The N [3], Na, and Al cosmic ray nuclei primary Φ_N^P, Φ_{Na}^P, and Φ_{Al}^P and secondary Φ_N^S, Φ_{Na}^S, and Φ_{Al}^S flux components, and their corresponding primary fractions Φ_N^P/Φ_N, Φ_{Na}^P/Φ_{Na}, and Φ_{Al}^P/Φ_{Al} at 6 GV, 100 GV, and 2 TV. As seen the primary fractions for all three fluxes increase with rigidity.

Nuclei flux	Primary	Secondary	Primary fraction,%		
			6 GV	100 GV	2 TV
Φ_N	$(0.092 \pm 0.002) \times \Phi_O$	$(0.61 \pm 0.02) \times \Phi_B$	31 ± 1	56 ± 1	77 ± 3
Φ_{Na}	$(0.036 \pm 0.003) \times \Phi_{Si}$	$(1.36 \pm 0.04) \times \Phi_F$	17 ± 2	35 ± 2	62 ± 12
Φ_{Al}	$(0.103 \pm 0.004) \times \Phi_{Si}$	$(1.04 \pm 0.03) \times \Phi_F$	43 ± 1	67 ± 1	78 ± 8

To examine the rigidity dependence of the sodium and aluminum fluxes with respect to heavy secondary cosmic rays, we use the fluorine flux Φ_F [7] as a characteristic secondary flux. The sodium to fluorine flux ratio Φ_{Na}/Φ_F and the aluminum to fluorine flux ratio Φ_{Al}/Φ_F were computed and are reported in Tables SV and SVI of the SM [16], respectively, as functions of rigidity with statistical and systematic errors.

To obtain the primary Φ_{Na}^P and secondary Φ_{Na}^S components in the Na flux $\Phi_{Na} = \Phi_{Na}^P + \Phi_{Na}^S$, a fit of Φ_{Na} to the weighted sum of a heavy primary cosmic ray flux, namely, silicon Φ_{Si} [6], and of a heavy secondary cosmic ray flux, namely, fluorine Φ_F [7], was performed above 6 GV. The fit yields $\Phi_{Na}^P = (0.036 \pm 0.003) \times \Phi_{Si}$ and $\Phi_{Na}^S = (1.36 \pm 0.04) \times \Phi_F$ with a $\chi^2/\text{DOF} = 19/36$, as shown in Fig. 3(a). Figure S6 of the SM [16] shows the result of this fit in terms of Φ_{Na}/Φ_{Si} and Φ_{Na}/Φ_F.
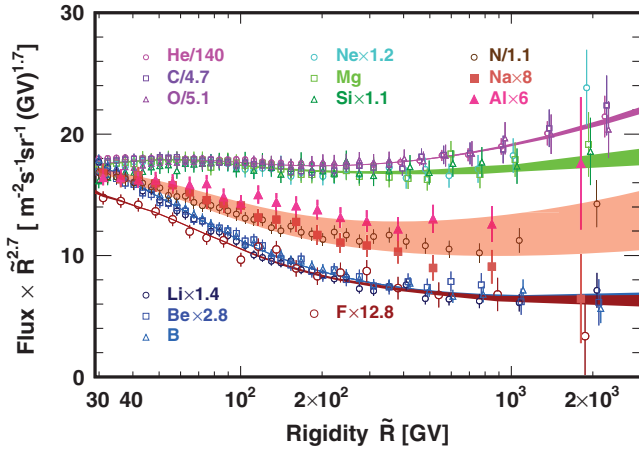
FIG. 4. The fluxes of cosmic nuclei measured by AMS as a function of rigidity from $Z = 2$ to $Z = 14$ above 30 GV. As seen, there are two classes of primary cosmic rays, He-C-O and Ne-Mg-Si, and two classes of secondary cosmic rays, Li-Be-B and F [7]. Nitrogen (N), sodium (Na), and aluminum (Al), belong to a distinct group and are the combinations of primary and secondary cosmic rays. For clarity, data points above 400 GV are displaced horizontally. For display purposes only, fluxes were rescaled as indicated. The shaded tan band on N, Na, and Al is to guide the eye.

Similarly, to obtain the primary Φ_{Al}^P and secondary Φ_{Al}^S components in the Al flux $\Phi_{Al} = \Phi_{Al}^P + \Phi_{Al}^S$, a fit of Φ_{Al} to the weighted sum of the silicon flux and the fluorine flux was performed above 6 GV. The fit yields $\Phi_{Al}^P = (0.103 \pm 0.004) \times \Phi_{Si}$ and $\Phi_{Al}^S = (1.04 \pm 0.03) \times \Phi_F$ with $\chi^2/\text{DOF} = 24/36$, as shown in Fig. 3(b). Figure S7 of the SM [16] shows the result of this fit in terms of Φ_{Al}/Φ_{Si} and Φ_{Al}/Φ_F.

As seen from Fig. 3, the contributions of the secondary component in both the sodium flux and the aluminum flux decrease with rigidity, and the contributions of the primary component increase with rigidity. The same dependence was also observed for the nitrogen flux Φ_N [3], see also Fig. S8 of the SM [16]. Table I details the primary Φ_N^P, Φ_{Na}^P, and Φ_{Al}^P and secondary Φ_N^S, Φ_{Na}^S, and Φ_{Al}^S components and also the primary fractions Φ_N^P/Φ_N, Φ_{Na}^P/Φ_{Na}, and Φ_{Al}^P/Φ_{Al} at different rigidities.

The observation that, similar to N [2,3], both the Na and Al fluxes can be fit over a wide rigidity range as the linear combinations of primary and secondary fluxes is a new and important result, which permits the direct determination of the Na/Si and Al/Si abundance ratios at the source, 0.036 ± 0.003 for Na/Si and 0.103 ± 0.004 for Al/Si, without the need to consider the Galactic propagation of cosmic rays. To study the effect of cosmic ray propagation on the Na/Si and Al/Si abundance ratio measurements at the source we used the models from Ref. [33]. The results are detailed in the SM [16] and show that the propagation effects on the Na/Si and Al/Si abundance ratio measurements at the source are negligible.

Figure 4 presents cosmic nuclei fluxes measured by AMS as a function of rigidity from $Z = 2$ to $Z = 14$. It shows that there are two classes of primary cosmic rays, He-C-O and Ne-Mg-Si, and two classes of secondary cosmic rays, Li-Be-B and F [7]. As seen from Fig. 4, N, Na, and Al belong to a distinct group and are the combinations of primary and secondary cosmic rays.

In conclusion, following the study of nitrogen, we have presented the precision measurement of the Na and Al fluxes as functions of rigidity from 2.15 GV to 3.0 TV, with detailed studies of the systematic errors. We found that Na and Al, together with N, belong to a distinct cosmic ray group and are the combinations of primary and secondary

cosmic rays. Similar to the N flux, which is well described by the sum of a primary cosmic ray component (proportional to the oxygen flux) and a secondary cosmic ray component (proportional to the boron flux), both the Na and Al fluxes are well described by the sums of a primary cosmic ray component (proportional to the silicon flux) and a secondary cosmic ray component (proportional to the fluorine flux). The fraction of the primary component increases with rigidity for the N, Na, and Al fluxes and becomes dominant at the highest rigidities. The Na/Si and Al/Si abundance ratios at the source, 0.036 ± 0.003 for Na/Si and 0.103 ± 0.004 for Al/Si, are directly determined independent of cosmic ray propagation. These are new and unexpected properties of cosmic rays.

---

[*] Also at Nikhef, 1098 XG Amsterdam, Netherlands.

[†] Also at ASI Space Science Data Center (SSDC), 00133 Roma, Italy.

[‡] Also at Policlinico S. Orsola-Malpighi, 40138 Bologna, Italy.

[1] I. A. Grenier, J. H. Black, and A. W. Strong, The nine lives of cosmic rays in galaxies, Annu. Rev. Astron. Astrophys. 53, 199 (2015); P. Blasi, The origin of galactic cosmic rays, Astron. Astrophys. Rev. 21, 70 (2013); A. W. Strong, I. V. Moskalenko, and V. S. Ptuskin, Cosmic-ray propagation and interactions in the galaxy, Annu. Rev. Nucl. Part. Sci. 57, 285 (2007); A. Castellina and F. Donato, Diffusion coefficient and acceleration spectrum from direct measurements of charged cosmic ray nuclei, Astropart. Phys. 24, 146 (2005); G. Jóhannesson et al., Bayesian analysis of cosmic ray propagation: Evidence against homogeneous diffusion, Astrophys. J. 824, 16 (2016).

[2] M. Aguilar et al., Precision Measurement of Cosmic-Ray Nitrogen and its Primary and Secondary Components with the Alpha Magnetic Spectrometer on the International Space Station, Phys. Rev. Lett. 121, 051103 (2018).

[3] M. Aguilar et al., The Alpha Magnetic Spectrometer (AMS) on the International Space Station: Part II-results from the first seven years, Phys. Rep. 894, 1 (2021). Note that in this Letter, we have used the He-C-O, Li-Be-B, Ne-Mg-Si, F, and N data covering the same collection time as Na and Al.

[4] M. Aguilar et al., Observation of the Identical Rigidity Dependence of He, C, and O Cosmic Rays at High Rigidities by the Alpha Magnetic Spectrometer on the International Space Station, Phys. Rev. Lett. 119, 251101 (2017).

[5] M. Aguilar et al., Observation of New Properties of Secondary Cosmic Rays Lithium, Beryllium, and Boron by the Alpha Magnetic Spectrometer on the International Space Station, Phys. Rev. Lett. 120, 021101 (2018).

[6] M. Aguilar et al., Properties of Neon, Magnesium, and Silicon Primary Cosmic Rays Results from the Alpha

Magnetic Spectrometer, Phys. Rev. Lett. **124**, 211102 (2020).

[7] M. Aguilar *et al.*, Properties of Heavy Secondary Fluorine Cosmic Rays: Results from the Alpha Magnetic Spectrometer, Phys. Rev. Lett. **126**, 081102 (2021).

[8] E. Juliusson, Charge composition and energy spectra of cosmic-ray nuclei at energies above 20 GeV per nucleon, Astrophys. J. **191**, 331 (1974).

[9] R. C. Maehl, J. F. Ormes, A. J. Fisher, and F. A. Hagen, Energy spectra of cosmic ray nuclei: $4 \le Z \le 26$ and $0.3 \le E \le 2$ GeV amu^{-1}, Astrophys. Space Sci. **47**, 163 (1977).

[10] C. D. Orth, A. Buffington, G. F. Smoot, and T. S. Mast, Abundances and spectra for cosmic-ray nuclei from lithium to iron for 2 to 150 GeV per nucleon, Astrophys. J. **226**, 1147 (1978).

[11] J. A. Lezniak and W. R. Webber, The charge composition and energy spectra of cosmic-ray nuclei from 3000 MeV per nucleon to 50 GeV per nucleon, Astrophys. J. **223**, 676 (1978).

[12] J. S. Young, P. S. Freier, C. J. Waddington, N. R. Brewster, and R. K. Fickle, The elemental and isotopic composition of cosmic rays—Silicon to nickel, Astrophys. J. **246**, 1014 (1981).

[13] J. J. Engelmann *et al.*, Charge composition and energy spectra of cosmic-ray nuclei for elements from Be to Ni- Results from HEAO-3-C2, Astron. Astrophys. **233**, 96 (1990).

[14] K. Lave *et al.*, Galactic cosmic-ray energy spectra and composition during the 2009–2010 solar minimum period, Astrophys. J. **770**, 117 (2013). This important paper provides measurements of Na and Al fluxes below 300 MeV/n.

[15] A. Kounine, The alpha magnetic spectrometer on the International Space Station, Int. J. Mod. Phys. E **21**, 1230005 (2012); S. Rosier-Lees, New results from AMS, in *Proceedings of Astroparticle Physics TEVPA/IDM, Amsterdam, 2014* (unpublished); S. Ting, The alpha magnetic spectrometer on the international space station, Nucl. Phys. B, Proc. Suppl. **243–244**, 12 (2013); S.-C. Lee, Latest results from AMS, in *Proceedings of the 20th International Conference on Supersymmetry and Unification of Fundamental Interactions (SUSY 2012), Beijing, 2012* (unpublished); M. Aguilar, The AMS experiment on the ISS, in *Proceedings of the XL International Meeting on Fundamental Physics, Centro de Ciencias de Benasque Pedro Pascual, 2012* (unpublished); S. Schael, Status of the AMS-02 experiment on the ISS, in *Proceedings of the 10th Symposium on Sources and Detection of Dark Matter and Dark Energy in the Universe, Los Angeles, 2012* (unpublished); B. Bertucci, The AMS-02 detector operation in space, Proc. Sci. EPS-HEP2011 (**2011**) 067; M. Incagli, Astroparticle Physiscs with AMS02, AIP Conf. Proc. **1223**, 43 (2010); R. Battiston, The antimatter spectrometer (AMS-02): A particle physics detector in space, Nucl. Instrum. Methods Phys. Res., Sect. A **588**, 227 (2008).

[16] See Supplemental material at http://link.aps.org/supplemental/10.1103/PhysRevLett.127.021101 for the details of the detector description, event selection, and results of the study of cosmic ray propagation effects; tabulated Na and Al fluxes, and the Na/Si, Al/Si, Na/F and Al/F ratios as functions of rigidity; and figures regarding detector layout, charge selection, Na and Al survival probabilities, the AMS N/O, Na/Si, Na/F, Al/Si, and Al/F flux ratios.

[17] K. Lübelsmeyer *et al.*, Upgrade of the Alpha Magnetic Spectrometer (AMS-02) for long term operation on the International Space Station (ISS), Nucl. Instrum. Methods Phys. Res., Sect. A **654**, 639 (2011).

[18] B. Alpat *et al.*, The internal alignment and position resolution of the AMS-02 silicon tracker determined with cosmic-ray muons, Nucl. Instrum. Methods Phys. Res., Sect. A **613**, 207 (2010).

[19] Y. Jia, Q. Yan, V. Choutko, H. Liu, and A. Oliva, Nuclei charge measurement by the Alpha Magnetic Spectrometer silicon tracker, Nucl. Instrum. Methods Phys. Res., Sect. A **972**, 164169 (2020).

[20] G. Ambrosi, V. Choutko, C. Delgado, A. Oliva, Q. Yan, and Y. Li, The spatial resolution of the silicon tracker of the Alpha Magnetic Spectrometer, Nucl. Instrum. Methods Phys. Res., Sect. A **869**, 29 (2017).

[21] V. Bindi *et al.*, Calibration and performance of the AMS-02 time of flight detector in space, Nucl. Instrum. Methods Phys. Res., Sect. A **743**, 22 (2014).

[22] J. Allison *et al.*, Recent developments in GEANT4, Nucl. Instrum. Methods Phys. Res., Sect. A **835**, 186 (2016); Geant4 developments and applications, IEEE Trans. Nucl. Sci. **53**, 270 (2006); S. Agostinelli *et al.*, GEANT4—a simulation toolkit, Nucl. Instrum. Methods Phys. Res., Sect. A **506**, 250 (2003).

[23] Q. Yan, V. Choutko, A. Oliva, and M. Paniccia, Measurements of nuclear interaction cross sections with the Alpha Magnetic Spectrometer on the International Space Station, Nucl. Phys. **A996**, 121712 (2020).

[24] M. Aguilar *et al.*, Precision Measurement of the Helium Flux in Primary Cosmic Rays of Rigidities 1.9 GV to 3 TV with the Alpha Magnetic Spectrometer on the International Space Station, Phys. Rev. Lett. **115**, 211101 (2015).

[25] M. Aguilar *et al.*, Precision Measurement of the Proton Flux in Primary Cosmic Rays from Rigidity 1 GV to 1.8 TV with the Alpha Magnetic Spectrometer on the International Space Station, Phys. Rev. Lett. **114**, 171103 (2015).

[26] M. Aguilar *et al.*, Precision Measurement of the Boron to Carbon Flux Ratio in Cosmic Rays from 1.9 GV to 2.6 TV with the Alpha Magnetic Spectrometer on the International Space Station, Phys. Rev. Lett. **117**, 231102 (2016).

[27] J. Alcaraz *et al.*, Leptons in near earth orbit, Phys. Lett. B **484**, 10 (2000).

[28] C. C. Finlay *et al.*, International Geomagnetic Reference Field: The eleventh generation, Geophys. J. Int. **183**, 1216 (2010); E. Thébault *et al.*, International geomagnetic reference field: The 12th generation, Earth Planets Space **67**, 79 (2015); Geomagnetic Field Modeling Working Group, IGRF-13 model, 2019, https://www.ngdc.noaa.gov/IAGA/vmod/igrf.html.

[29] J. Berdugo, V. Choutko, C. Delgado, and Q. Yan, Determination of the rigidity scale of the Alpha Magnetic Spectrometer, Nucl. Instrum. Methods Phys. Res., Sect. A **869**, 10 (2017).

[30] G. D. Lafferty and T. R. Wyatt, Where to stick your data points: The treatment of measurements within wide bins, Nucl. Instrum. Methods Phys. Res., Sect. A **355**, 541 (1995). We have used Eq. (6) with $\tilde{R} \equiv x_{lw}$.

[31] D. Maurin, F. Melot, and R. Taillet, A database of charged cosmic rays, Astron. Astrophys. **569,** A32 (2014).

[32] M. J. Boschini *et al.*, Inference of the local interstellar spectra of cosmic-ray nuclei $Z \leq 28$ with the GALPROP–HELMOD framework, Astrophys. J. Suppl. Ser. **250,** 27 (2020).

[33] M. Aguilar *et al.*, Properties of Iron Primary Cosmic Rays: Results from the Alpha Magnetic Spectrometer, Phys. Rev. Lett. **126,** 041104 (2021).

[34] Including computing support on the JARA partition of the RWTH Aachen supercomputer.